SUPPLEMENTARY FIGURES

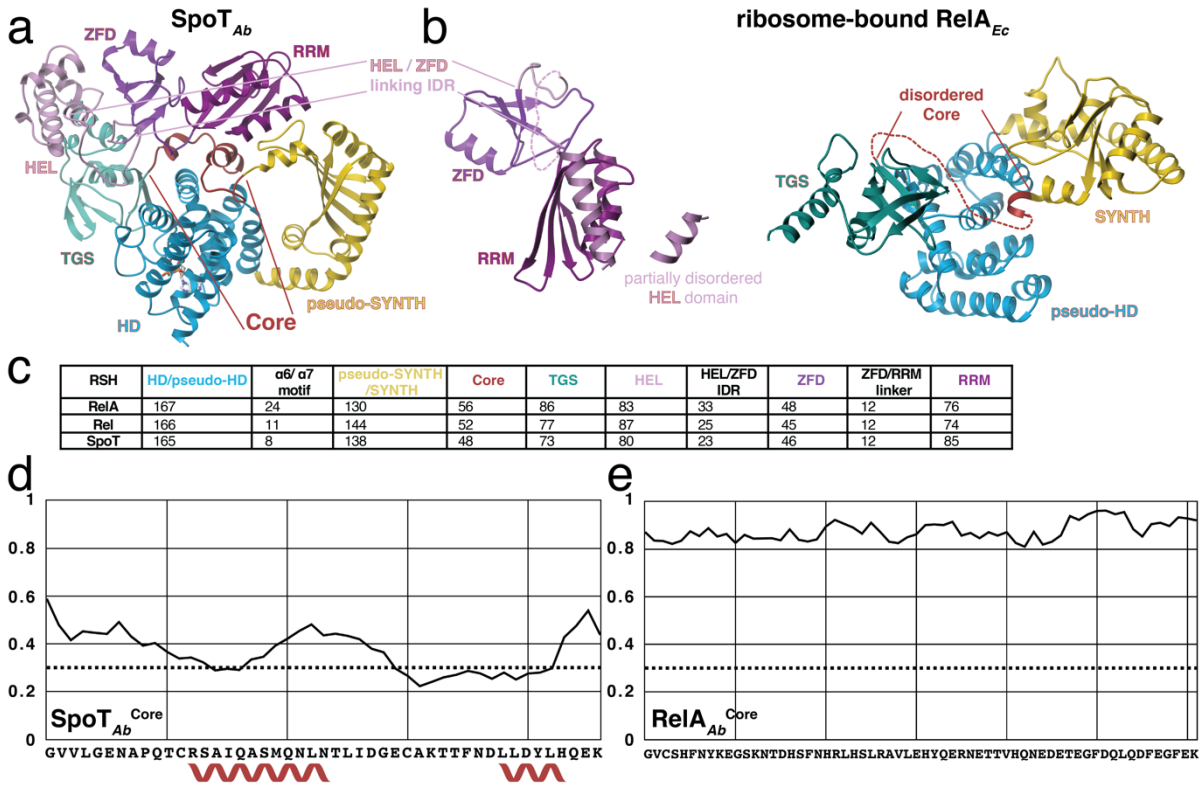

RSH	HD/pseudo-HD	α6/ α7 motif	pseudo-SYNTH /SYNTH	Core	TGS	HEL	HEL/ZFD IDR	ZFD	ZFD/RRM linker	RRM
RelA	167	24	130	56	86	83	33	48	12	76
Rel	166	11	144	52	77	87	25	45	12	74
SpoT	165	8	138	48	73	80	23	46	12	85

Supplementary Fig. 1. The linker regions connecting α-helices α6 and α7, SYNTH (pseudo-SYNTH) with TGS, and HEL with ZFD appear as highly flexible regions in the structures of free SpoT$_{Ab}$ as well as *E. coli* RelA bound starved ribosomal complex, related to Fig. 2. Cartoon representation of the structures of SpoT$_{Ab}$ (**a**) and *E. coli* RelA (Brown et al., 2016) in the conformation bound to 70S ribosomes and uncharged A-site tRNA (**b**). The intrinsically disordered linker regions that are not visible in the structures are highlighted in the figures and the individual domains are coloured as on Figure 2A. (**c**) Average length of the different domains and interdomain regions of bifunctional Rel, and the monofunctional RelA and SpoT. Analysis of the intrinsic disorder propensity of the Core domain of SpoT$_{Ab}$ (**d**) vs RelA$_{Ab}$ (**e**) calculated with flDPnn. The two α-helices observed in the Core of SpoT$_{Ab}$ match the two stretches predicted by flDPnn with low disordered content. The comparison of both Core regions suggests RelA$_{Ab}$ Core is significantly more disordered than that of SpoT$_{Ab}$.

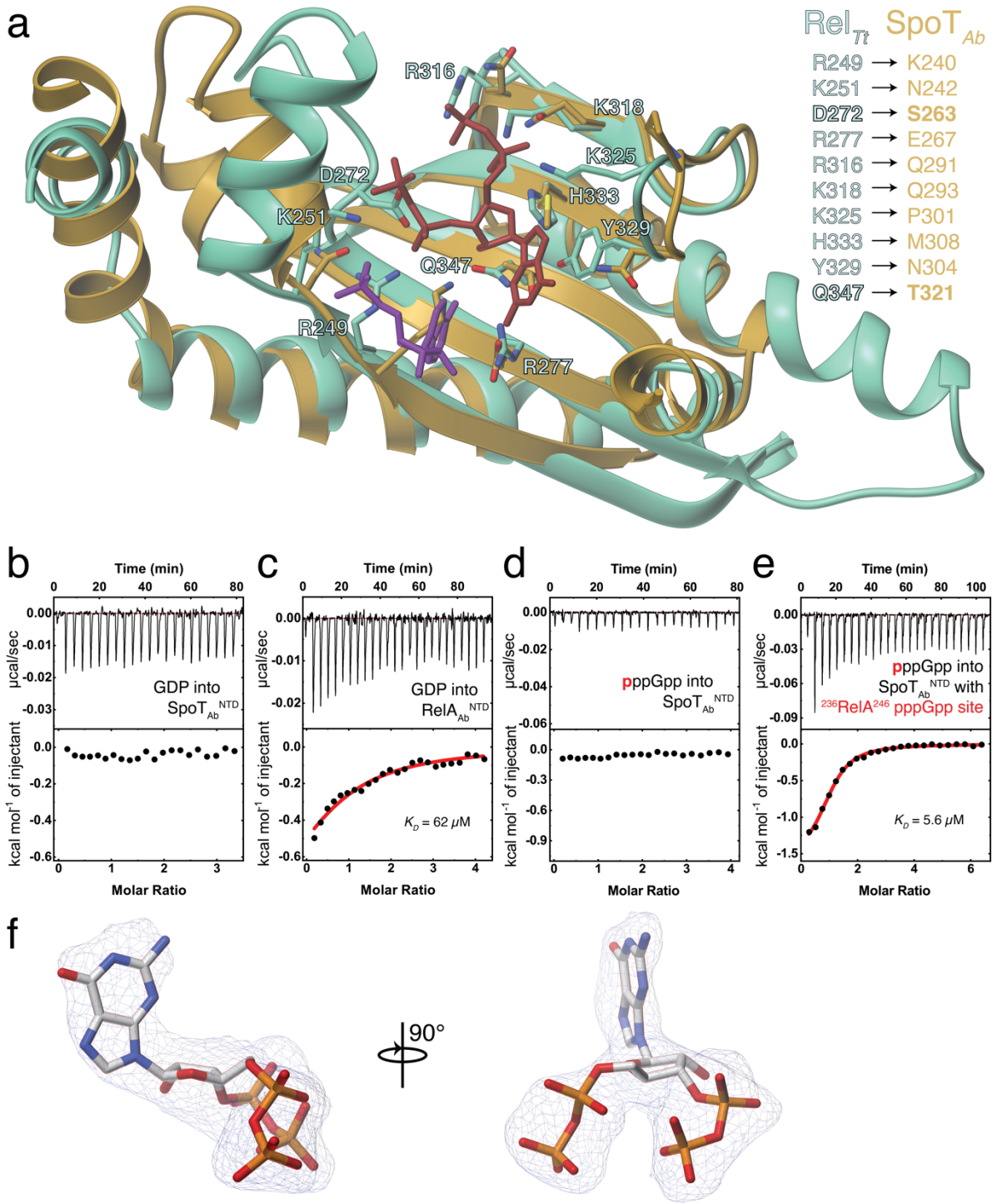

Supplementary Fig. 2. SpoT$_{Ab}$ is a monofunctional (p)ppGpp hydrolase with a degenerated pseudo-SYNTH domain, related to Fig. 2.
(**a**) Superposition of the pseudo-SYNTH domain of SpoT$_{Ab}$ (in gold) onto the SYNTH domain of *T. thermophilus* Rel (Rel$_{Tt}$) bound to ppGpp and AMP (in green). While the overall topology of the domain is conserved, a large number of substitutions in the nucleotide binding sites precludes substrate binding and catalysis of the pyrophosphate transfer. The crucial conserved Y that stacks with the guanine base of GDP and GTP is substituted to N, while the R residues that stacks with adenine (R249 and R277 in Rel$_{Tt}$) changed to K and E, respectively. Finally, catalytic residues D, E and Q residues involved Mg^{2+} coordination and hydrolysis changed to S263, 2319 and T321, respectively. ITC titrations of GDP into either SpoT$_{Ab}^{NTD}$ (**b**) or

RelA$_{Ab}^{NTD}$ (**c**). ITC titration of pppGpp into SpoT$_{Ab}^{NTD}$ (**d**)and SpoT$_{Ab}^{NTD}$ with a grafted pppGpp-biding site of RelA$_{Ab}$, ^{236}RelA^{246} (**e**). In both cases the enzymes are supplemented with 1 mM APCPP, 1 mM GDP, and 10 mM EDTA. (**f**) Unbiased mFo-DFc electron density map of ppGpp bound to SpoT$_{Ab}$, after refinement with Buster/TNT and omitting ppGpp.

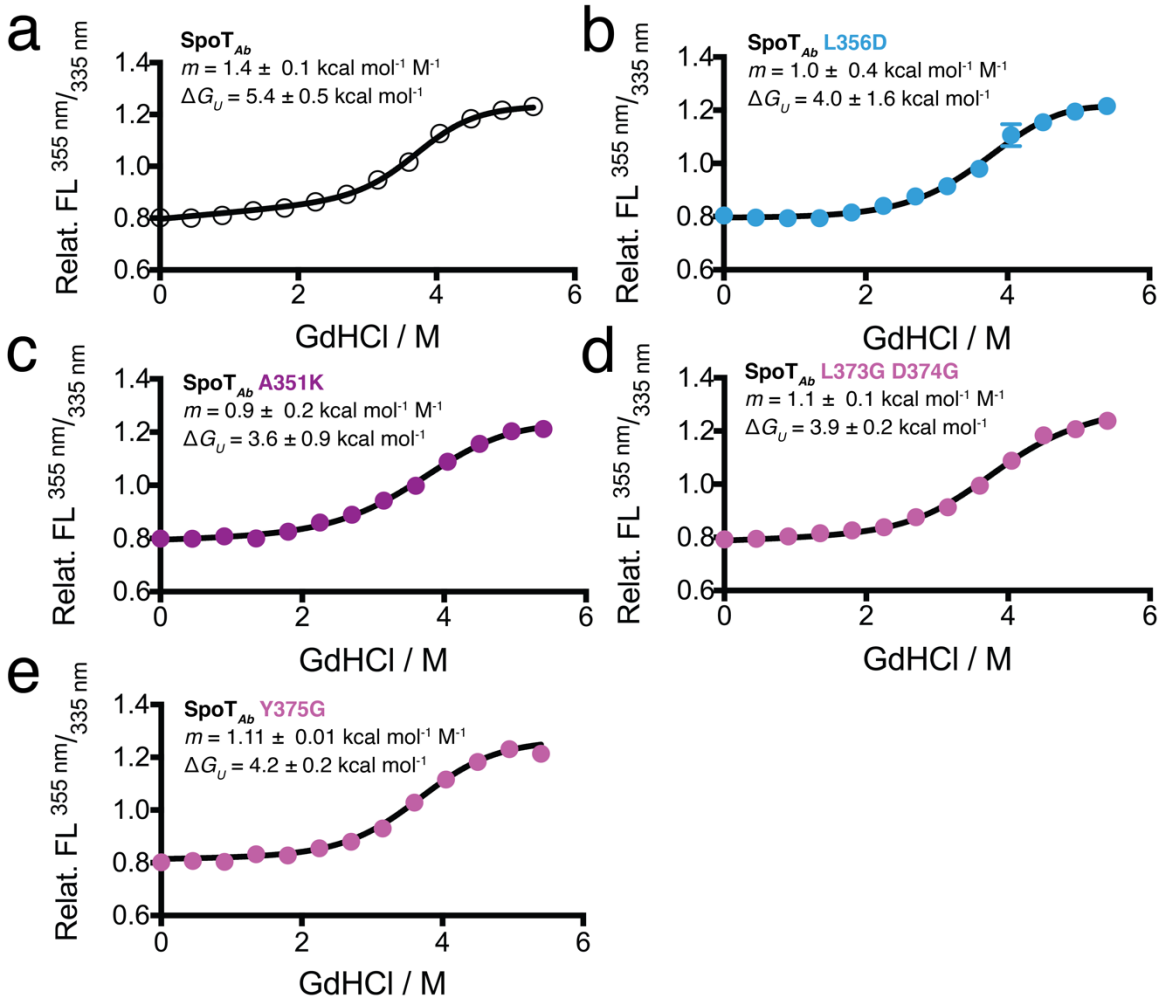

Supplementary Fig. 3. Effects of amino acid substitutions on the structural stability of SpoT$_{Ab}$, related to Fig. 4. Thermal denaturation profiles monitored by far UV CD spectrum at 222 nm probing the α–helical content of wild-type SpoT$_{Ab}$ (**a**) as well as substituted variants (**b**-**e**).

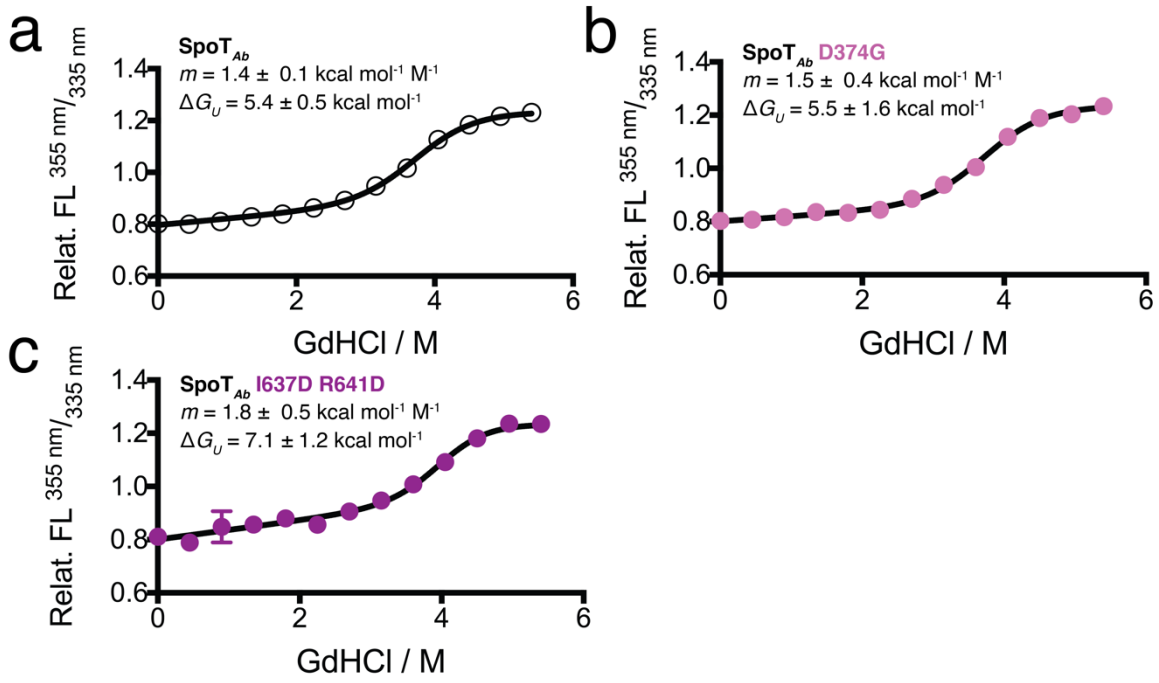

Supplementary Fig. 4. Effects of amino acid substitutions on the structural stability of SpoT$_{Ab}$, related to Fig. 5. Thermal denaturation profiles monitored by far UV CD spectrum at 222 nm probing the α–helical content of wild-type SpoT$_{Ab}$ (**a**) as well as substituted variants (**b** and **c**).